Bull. Inst. Chem. Res., Kyoto Univ., Vol. 53, No. 2, 1975

# Effect of Through-Focusing on the Bright and Dark Field Molecular Images in High Resolution Electron Microscopy

Kazuo ISHIZUKA and Natsu UYEDA

*Received May 16, 1975*

The anticipated effect of through-focusing on the molecular images was investigated with the computer simulated high resolution electron micrographs of the thin crystal of chlorinated-Cu-phthalocyanine. It was demonstrated that the molecular image reflecting the specimen structure will appear only at one focus position of through-focusing in the bright field mode for 500 kV electrons with the spherical aberration coefficient $C_s$ of 1.0 and 1.8 mm. While in the dark field mode, only the heavy atoms in the molecule could be detected at the best focus position of through-focusing. For 100 kV electrons (with $C_s$=1.4 mm), the simulated images did not resolve the molecular details in both the bright and the dark field modes, but the bright field mode was superior to the dark field one in a sense that the general molecular shape could be recognized at the beat focus.

## I. INTRODUCTION

Recent progress in electron microscopy such as the developments of the condensor-objective lens by Ruska,[1] and of the vibration, drift and contamination free system has facilitated the high resolution work of the order of Angstrom. With the transmission electron microscope of the 100 kV class, the direct observations of some atoms or atomic clusters have been reported.[2~9]

The image formation and the effect of a spherical aberration of the electron lens was discussed by Scherzer[10] on the basis of phase contrast. Some numerical calculations of atomic contrast based on a kinematical approximation were carried out by Eisenhandler and Siegel,[11] Misell,[12] and Uyeda and Ishizuka.[13] Siegel[14] simulated the brominated organic molecules at their greatest contrast in the kinematical approximation. Moodie and his coworkers[9,15] synthesized the lattice images of various oxides for 100 kV electrons on the basis of $n$-beam dynamical theory. Cowley[7,16] proposed a semi-quantitative method to interpret the bright and the dark field image intensities in terms of the phase grating approximation.[17]

As is well known, the electron waves scattered in large angles should contribute to the image formation as well as those in small angles in order for the images to be resolved to give molecular details. It was shown in the previous paper[13] that the remarkable improvement in resolution of the bright field image may be obtained by the elevation of the accelerating voltage of electrons up to 500 kV and a reasonable spherical aberration coefficient as reported by Kobayashi *et al.*[18]

* 石塚和夫, 植田 夏 : Laboratory of Crystal and Powder Chemistry, Institute for Chemical Research, Kyoto University, Uji, Kyoto.

In the present report, the molecular images of both the bright and the dark field modes are simulated intensively for the electron-optical conditions such as the spherical aberration coefficient $C_s$=1.0 and 1.8 mm for 500 kV electrons, which will be compared with the simulation of similar images for 100 kV electrons of conventional instruments. Since the simulations are based on the kinematical approximation, they are to show the ultimate resolution which can be achieved with an idealized specimen as thin as a few unit cells.

## II. THEORETICAL

The intensity of a bright field image $I_{BF}(\boldsymbol{r}_i)$ and a dark field image $I_{DF}(\boldsymbol{r}_i)$, in which the transmitted wave is let through and cut-off by an aperture, respectively, can be expressed with an amplitude $\phi_i(\boldsymbol{r}_i)$ of the scattered wave expected to appear at the image plane;

$$I_{BF}(\boldsymbol{r}_i)=\frac{1}{M^2}|1-i\phi_i(\boldsymbol{r}_i)|^2$$

$$=\frac{1}{M^2}\{1+2\cdot\mathrm{Im}[\phi_i(\boldsymbol{r}_i)]+|\phi_i(\boldsymbol{r}_i)|^2\}, \tag{1}$$

$$I_{DF}(\boldsymbol{r}_i)=\frac{1}{M^2}|\phi_i(\boldsymbol{r}_i)|^2, \tag{2}$$

where $\boldsymbol{r}_i$ is a coordinate on the image plane, $M$ is the magnification of a microscope, and $\phi_i(\boldsymbol{r}_i)$ can be described by the Fourier transform within the reciprocal space $\boldsymbol{h}$ as follows;

$$\phi_i(\boldsymbol{r}_i)=\lambda\int F(\boldsymbol{h})\cdot\exp\{-i\chi(h)\}\cdot A(h)\cdot\exp\{-2\pi i\boldsymbol{h}(\boldsymbol{r}_i/M)\}\,\mathrm{d}\boldsymbol{h}. \tag{3}$$

In the kinematical approximation, $F(\boldsymbol{h})$ is the Fourier transform of the two-dimensional projection of the electric potential distribution in the scattering object. $A(h)$ is the aperture function which mathematically describes the physical aperture with the value of either one or zero. $\chi(h)$ is an aberration function expressed as follows;

$$\chi(h)=(2\pi/\lambda)\{(\Delta f/2)(\lambda h)^2-(C_s/4)(\lambda h)^4\}, \tag{4}$$

where $C_s$ is the coefficient of spherical aberration of an objective lens, $\Delta f$ the defocusing value and $\lambda$ the wavelength of electrons. The scattering angle $\alpha$ is related to $h$ by $h=2\cdot\sin(\alpha/2)/\lambda\simeq\alpha/\lambda$, *i.e.*, $\alpha\simeq\lambda h$.

A typical features of the aberration function can be seen in Fig. 1, where $C_s$=1.0 mm, $\lambda$=0.01421 Å (500 kV electrons) for various defocuses. Image change may be anticipated in both the bright and the dark field modes, because the amplitude $\phi_i$ suffers the phase shift by $\exp\{-i\chi\}$ due to the aberration on the Fourier component $F(\boldsymbol{h})$ as indicated in Eq. (3). This raises one of the inevitable problems to select the best image reflecting the structure of specimen molecule out of many micrographs, when one intends to determine the molecular structure directly from its image alone. According to Rayleigh's rule,[19] the quantity of image is not seriously affected by the phase change if the amount is less than a quarter of the wavelength or $|\chi|\leq\pi/2$. Therefore, the best image can be expected at the defocus of about 400 Å with the aperture angle $\alpha_{max}=0.85\times10^{-2}$ rad. for this electron-optical conditions.

In the bright field image of a weak scattering object for which $|\phi_i|\ll1$ (kinematical approximation), the interference term (*i.e.*, $\mathrm{Im}[\phi_i]$) for the transmitted and scattered

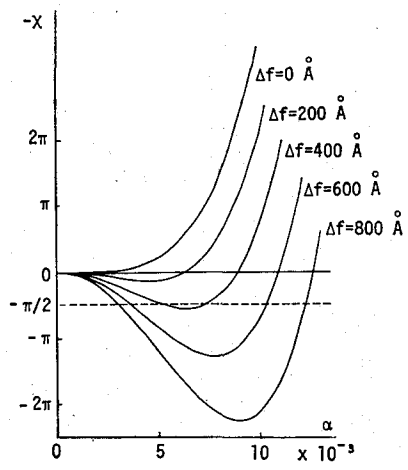


Fig. 1. Characteristics of the aberration function for 500 kV electrons with $C_s$=1.0 mm. The best focus will be obtained at the defocus of about 400 Å.

waves at the image plane mostly contributes to the image intensity, and thus the linear relation between the image intensity and the scattering amplitude $\phi_i$ makes the interpretation of image simple. On the contrary, in the dark field image the intensity is expressed by a square of the magnitude of $\phi_i$ (*i.e.*, $|\phi_i|^2$), and thus the interpretation of the image will become difficult by the following reasons: firstly, the contrast is exaggerated by the square of the scattering power, and secondly, the phase information of $\phi_i$ is lost when the image is recorded. For example, a negative value of the amplitude gives rise to a positive intensity (a ghost peak) which can not be discriminated from the ordinary peaks particularly when an original structure in unknown.

It must be noted that either the bright or the dark field images takes no advantage as far as the contrast (signal to noise ratio) is considered. The recording of the image is a quantum mechanical process, therefore the fluctuation in $N$ electrons will be $\sqrt{N}$ by Poisson's law. With an exposure $E$, the signal and the noise in the background are expressed as $|\phi_i|E$ and $\sqrt{E}$, respectively, for the bright field image, and thus the S/N ratio is equal to $|\phi_i|\sqrt{E}$. For the dark field image, the signal and its fluctuation are $|\phi_i|^2E$ and $\sqrt{|\phi_i|^2E}$, respectively, then the S/N ratio becomes also $|\phi_i|\sqrt{E}$. A low contrast specimen has a small S/N ratio for a fixed exposure in both the bright and the dark field images, therefore the organic molecules mostly composed of light atoms such as carbon, nitrogen and oxygen will only have the low contrast, high noise images. In order to overcome this difficulty, thin crystalline films of several unit cells piled in the thickness direction may be utilized to increase $|\phi_i|$ even for the low exposure which is necessary to avoid another difficulty such as radiation damages.

## III. RESULTS AND DISCUSSION

The molecular images were synthesized for hexadecachloro-Cu-phthalocyanine (Fig. 2 (a)), which is crystallized to assume a monoclinic form with the crystal data:[6]

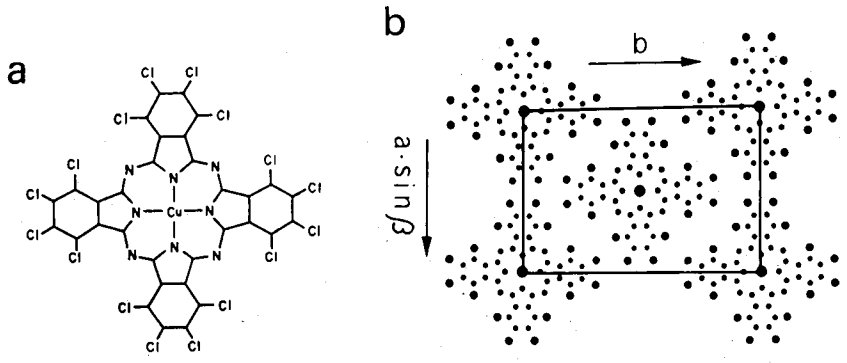


Fig. 2. Schematic representations of a model structure. a: Molecular structure of hexadecachloro-Cu-phthalocyanine. b: Crystal arrangement of the specimen projected along the $c$-axis.

$$a=19.62\ \text{Å},\quad b=26.04\ \text{Å},\quad c=3.76\ \text{Å},\quad \beta=116.5°.$$

The molecular image expected is schematically shown in Fig. 2 (b), which is a projection of the crystal along the $c$-axis. The symmetry of the image will be a plane group *cmm*. It is assumed that the kinematical approximation holds for the wave scattered from the specimen. Actually, the specimen of one unit cell in the thickness is assumed for simplicity in the following calculation. Then, the structure amplitudes $F(\boldsymbol{h})$ were calculated from the atomic scattering factors $f_j(\boldsymbol{h})$[20] and atomic parameters $\boldsymbol{r}_j$ as follows;

$$F(\boldsymbol{h})=\frac{1}{\sqrt{1-\beta^2}}\sum_j f_j(\boldsymbol{h})\cdot\exp\{2\pi i\boldsymbol{h}\boldsymbol{r}_j\}$$

where $1/\sqrt{1-\beta^2}$ is a relativistic correction factor with $\beta=v/c$ (1.979 for 500 kV electrons). A normal illumination is also assumed for both the bright and the dark field modes. The aperture function has the value of unity at $\alpha\leq\alpha_{\max}$ for the bright field mode, and $\alpha_{\min}\leq\alpha\leq\alpha_{\max}$ for the dark field one, where $\alpha_{\max}$ is selected to cut-off the scattered waves heavily degraded by the aberration and $\alpha_{\min}$ to stop the transmitted wave. In the following description, the quantity $s$ defined by $s=h/2\simeq\alpha/2\lambda$ will also be used instead of $\alpha$, then $s_{\min}=\alpha_{\min}/2\lambda$ and $s_{\max}=\alpha_{\max}/2\lambda$.

For 500 kV electrons with $C_s=1.0$ mm and $s_{\max}=0.31$ Å$^{-1}$, the images were synthesized with a series of defocusing values taken at 100 Å intervals. Some of the serial results are shown in Fig. 3, where the defocusing values are indicated under each figure. Obviously, the molecular details can be seen at $\Delta f=400$ Å, although the peaks for carbon and nitrogen atoms are not discriminated. The contrast was estimated to be 14% for heavy atoms and 4% for light atoms. The through-focusing gives rise to a considerable variation in contrast distribution forming completely wrong structures. The lowest contrast image was obtained at about $\Delta f=200$ Å, for which the transfer function for the bright field mode takes small values in the widest region. The simulated images near the best focus are shown in Fig. 4, where the molecular configuration is clearly observed in the images at the defocus value from 360 Å to 460 Å.[21]

The dark field images based on the elastically scattered electrons were synthesized with the aperture function of $s_{\min}=0.01$ and $s_{\max}=0.31$ Å$^{-1}$. Figure 5 shows the results of

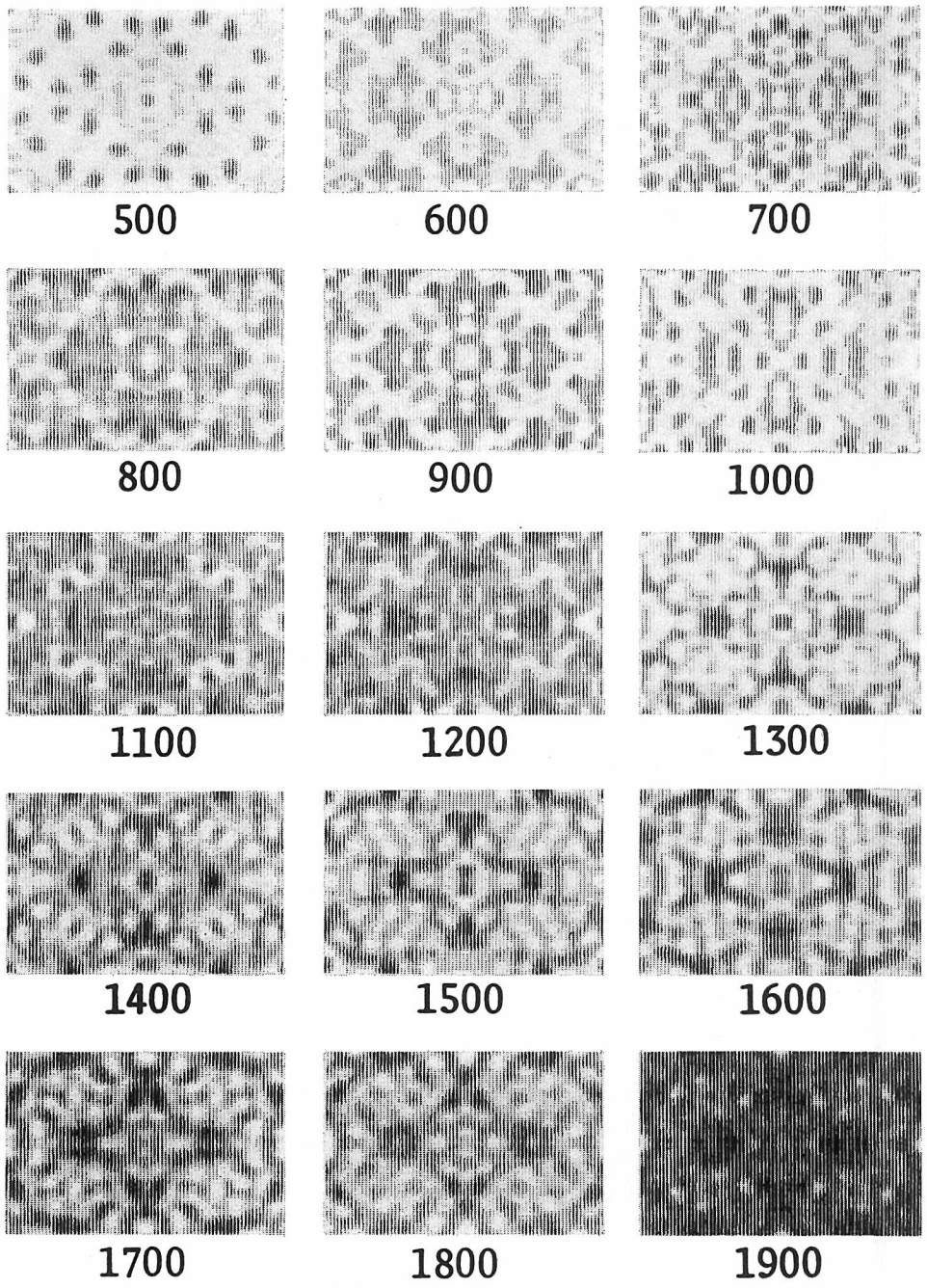


Fig. 3. Some results of a through-focusing calculation of the bright field image for 500 kV electrons with $C_s$=1.0 mm ($s_{msx}$=0.31 Å$^{-1}$). The defocus values are shown under each image. The best image is obtained at $\Delta f$=400 Å, where the shape of *iso*-indole rings as well as the heavy atoms are clearly observed.

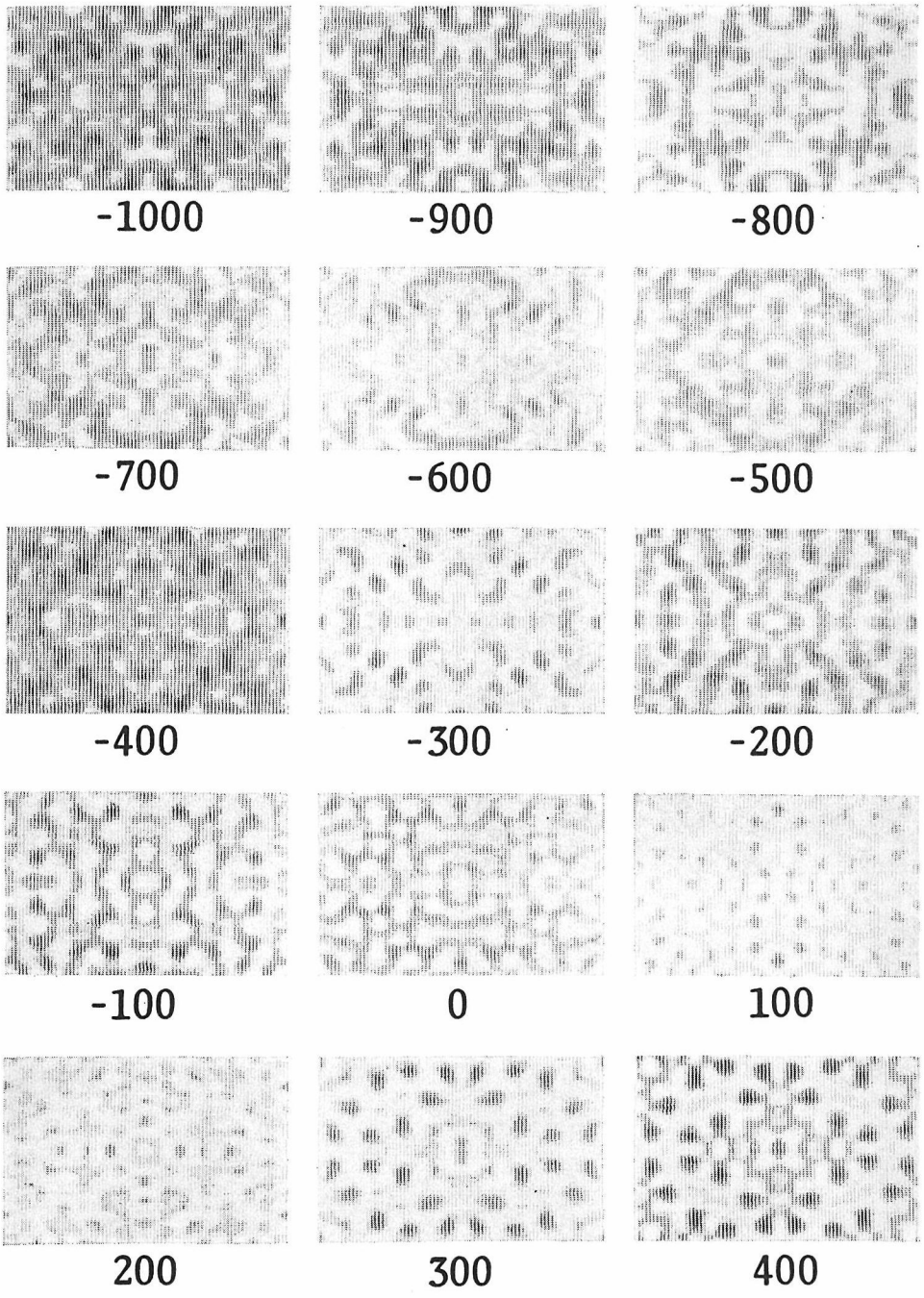


Fig. 3. (Cont.)

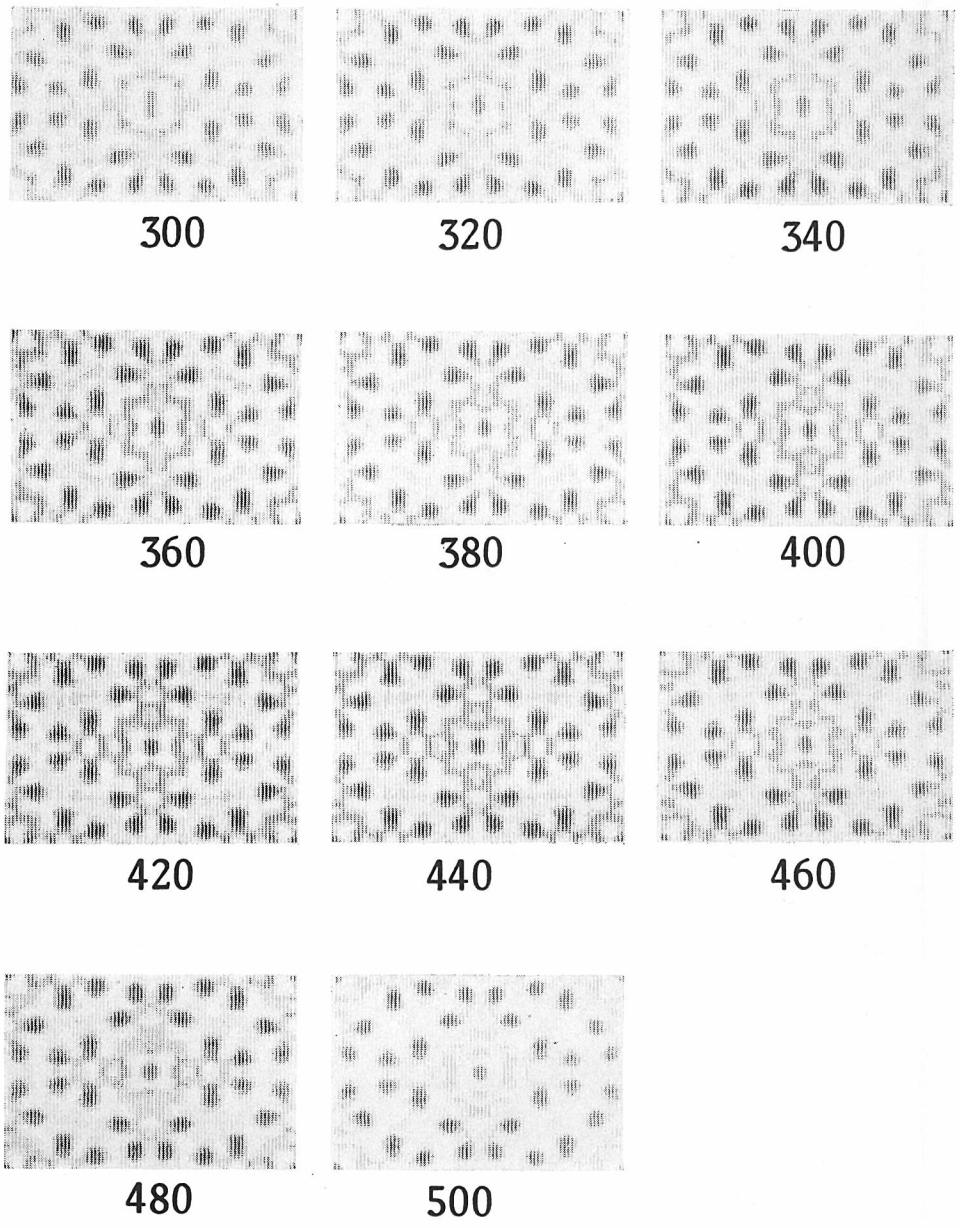


Fig. 4. Some bright field molecular images simulated in the vicinity of the best focus with $C_s = 1.0$ mm for 500 kV electrons. The molecular configuration is clearly observed in the images at the defocus values from 360 to 460 Å.

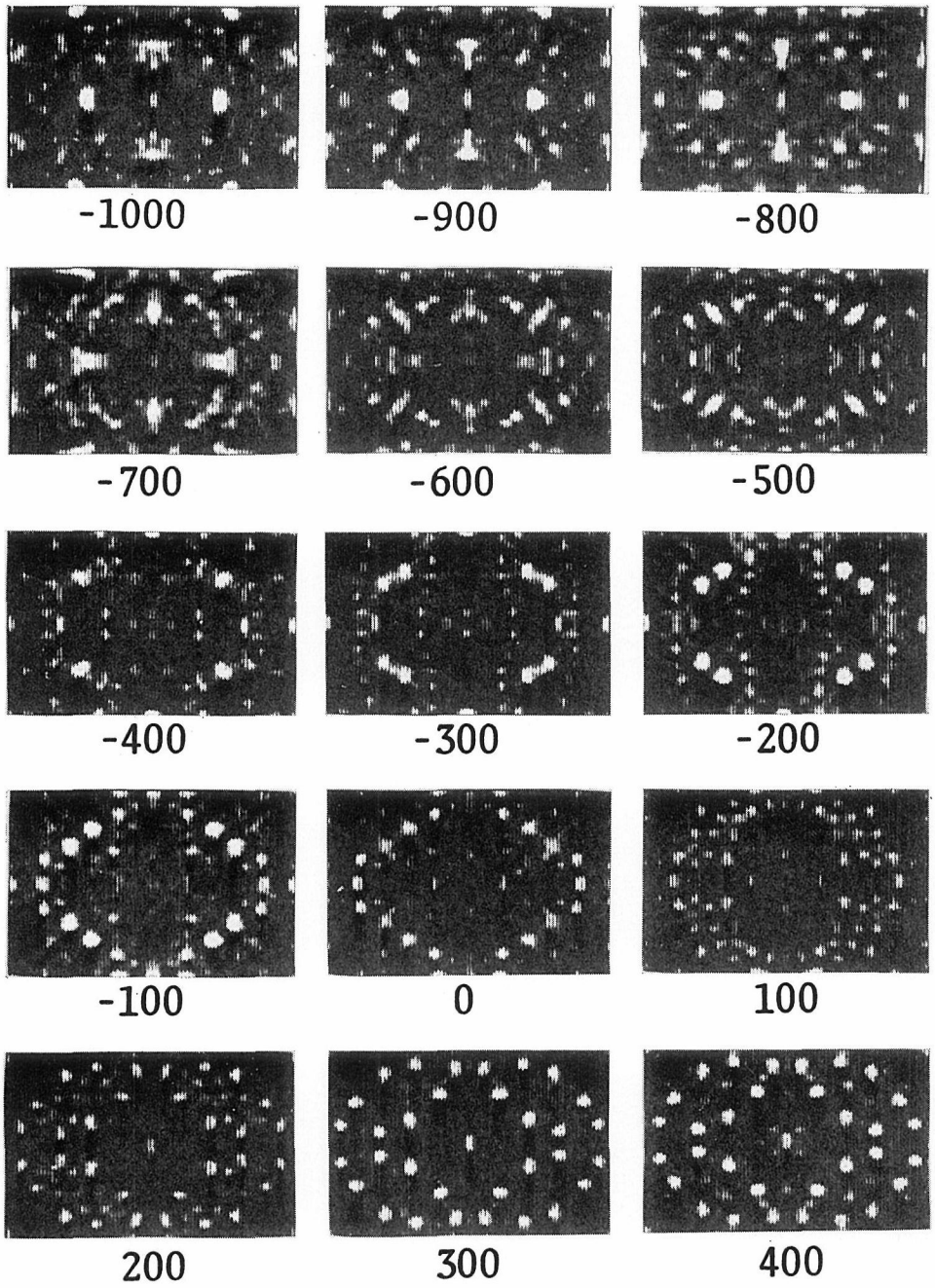


Fig. 5. Simulated molecular images of the dark field mode for 500 kV electrons with $C_s$ =1.0 mm ($s_{min}$=0.01 and $s_{max}$=0.31 Å$^{-1}$). The best image is obtained around $\Delta f$=300 Å, where only the heavy atoms can be detected.

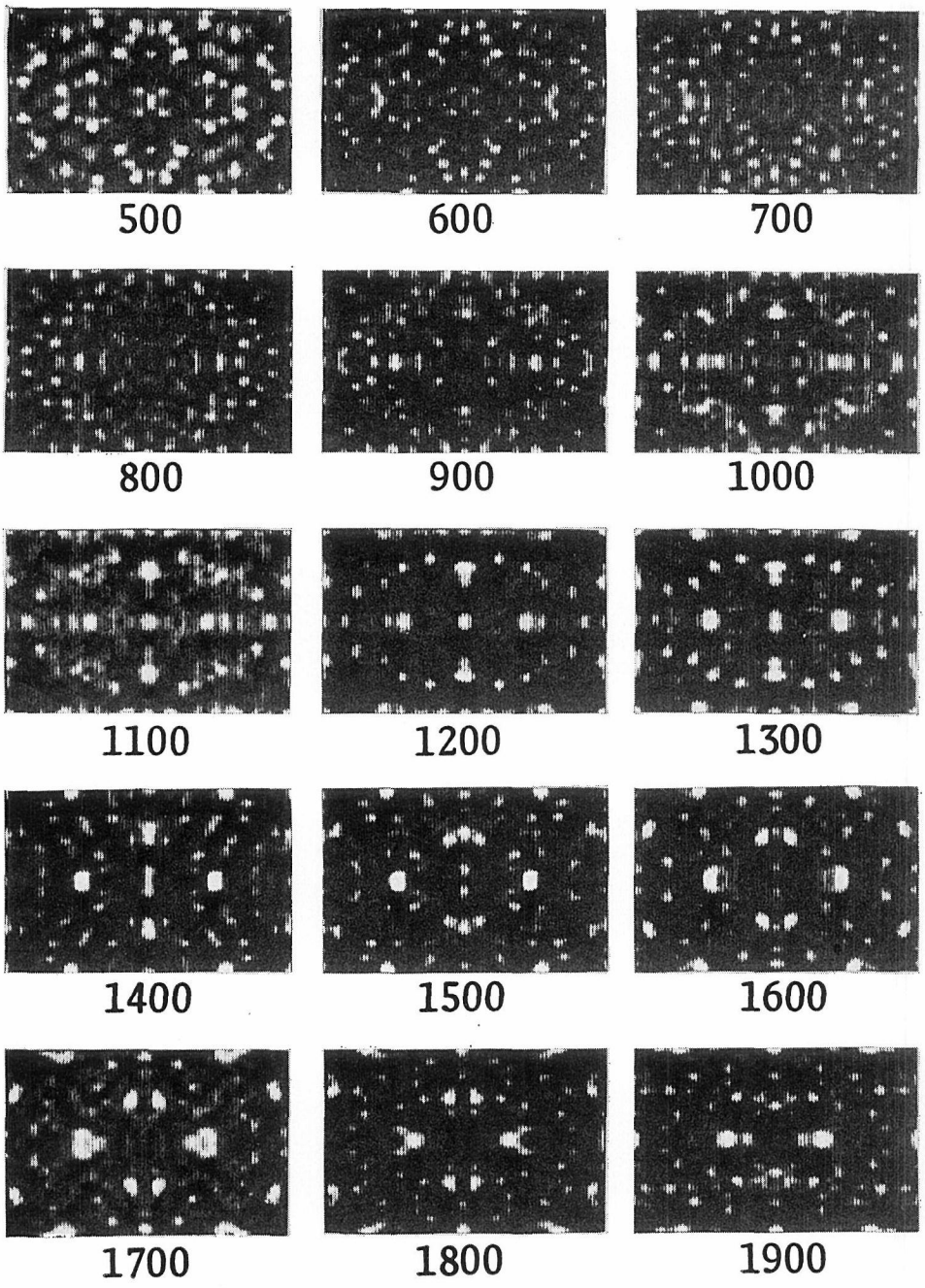
500
600
700
800
900
1000
1100
1200
1300
1400
1500
1600
1700
1800
1900

Fig. 5. (Cont.)

through-focusing performed with the defocusing intervals of 100 Å. The heavy atoms can be recognized with higher contrast than ghost peaks at the defocusing values of 300 and 400 Å, while the light atoms are hardly discriminated. Moreover, some ghost peaks even in those images are observed with greater intensities than the true peaks corresponding to the light atoms. At other defocus points, the highest peak sometimes does not correspond to the true atomic position but is often located between the heavy atom positions, as can be seen in the images at $\Delta f=-800$, $-100$, *etc.* The origin of such ghost peaks lies in the interference of the ripples around atomic images, and subsequent squaring of the magnitude into the intensity. It must be pointed out that the contrast of the molecular image shows considerable changes with the defocusing also in the case of the dark field image. It is easily surmised that the interpertation of the image will become more difficult for other dark field mode (*e.g.* displaced aperture dark field mode) because of the asymmetry in the propagation of scattered waves which contribute to the image formation. Moreover, in the dark field image formation the inelastically scattered electrons have the same important contribution to its intensity as the elastically scattered ones even for a thin phase object in contrast to the bright field mode, where the elastic electrons derive an advantage from the interference with the transmitted wave. Then, the effect of chromatic aberration with the inelastic electons on the image formation must be taken into account.

Another series of images were synthesized for 500 kV electrons with a spherical aberration coefficient $C_s=1.8$ mm, which is about twice the value of the former case. The aperture angle was set as $0.75\times10^{-2}$ rad., *i.e.*, $s_{max}=0.264$ Å$^{-1}$. The results of some serial computed images of the bright field mode are shown in Fig. 6 and the images near the best focus in Fig. 7. The best image was obtained at $\Delta f=550$ Å, and the torelable images were observed between the defocus of 450 and 610 Å. While the heavy atoms were clearly observed, the *iso*-indole rings composed of light atoms were slightly deformed even in the best image. The dark field images calculated with $s_{min}=0.01$ and $s_{max}=0.264$ Å$^{-1}$ were shown in Fig. 8. The heavy atoms can be recognized at the defocus values of 500 and 600 Å. It may be noted that when the spherical aberration coefficient is degraded from 1.0 to 1.8 mm, the overall feature of the serial images was shifted to the under-focus side by the defocus of about 100～200 Å.

The above results of 500 kV electrons may be compared with the images synthesized for 100 kV electrons with the spherical aberration coefficient ($C_s=1.4$ mm) attained in the conventional electron microscopes. In this case $\alpha_{max}$ is set to be $1.08\times10^{-2}$ rad. ($s_{max}=0.146$ Å$^{-1}$). The results of the bright field images of some serial defocus values are shown in Fig. 9, where in all cases even the heavy atoms can not be discriminated. The best image was obtained at the defocus value of about 900 Å in a sense that the general molecular shape like a four-leaf clover is recognized anyhow. It can be appreciated that the effect of the interference between the copper and the neighbor atoms weaken the contrast at the center of the molecule. The dark field images were synthesized with $s_{min}=0.01$ and $s_{max}=0.146$ Å$^{-1}$, some of which are shown in Fig. 10. It must be noted that in all cases the highest contrast peak does not appear at the heavy atom positions. At the focus of about 900 Å, the molecular shape can be recognized, but the ghost peaks of high intensity appear in this image.

It may be concluded that the image reflecting the molecular structure will appear in the through-focusing with a fine defocusing intervals for 500 kV electrons in the bright

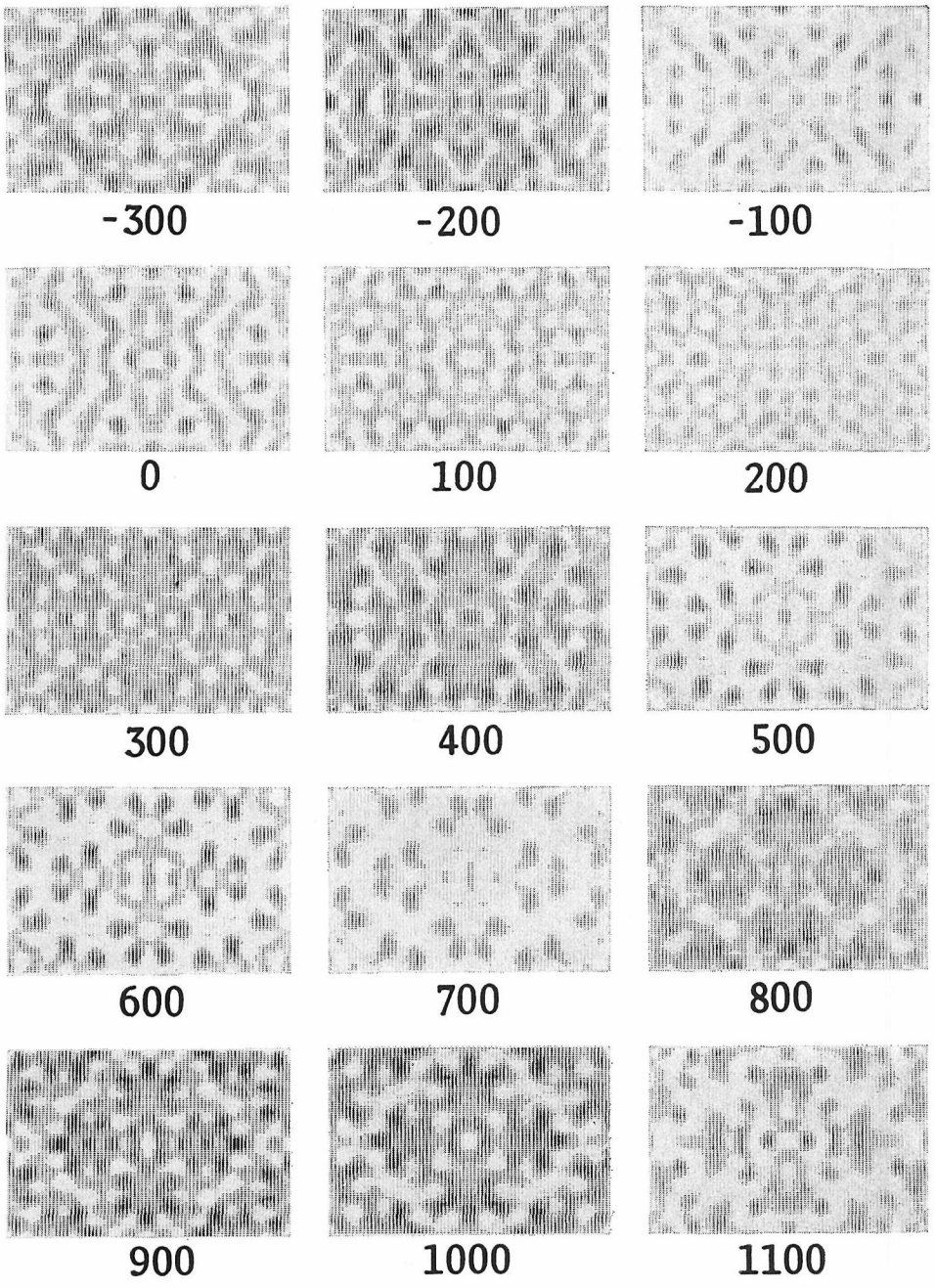


Fig. 6. Some results of the bright field images synthesized with $C_s$=1.8 mm for 500 kV electrons ($s_{max}$=0.264 Å$^{-1}$). The best image is obtained between the defocus values of 500 and 600 Å.

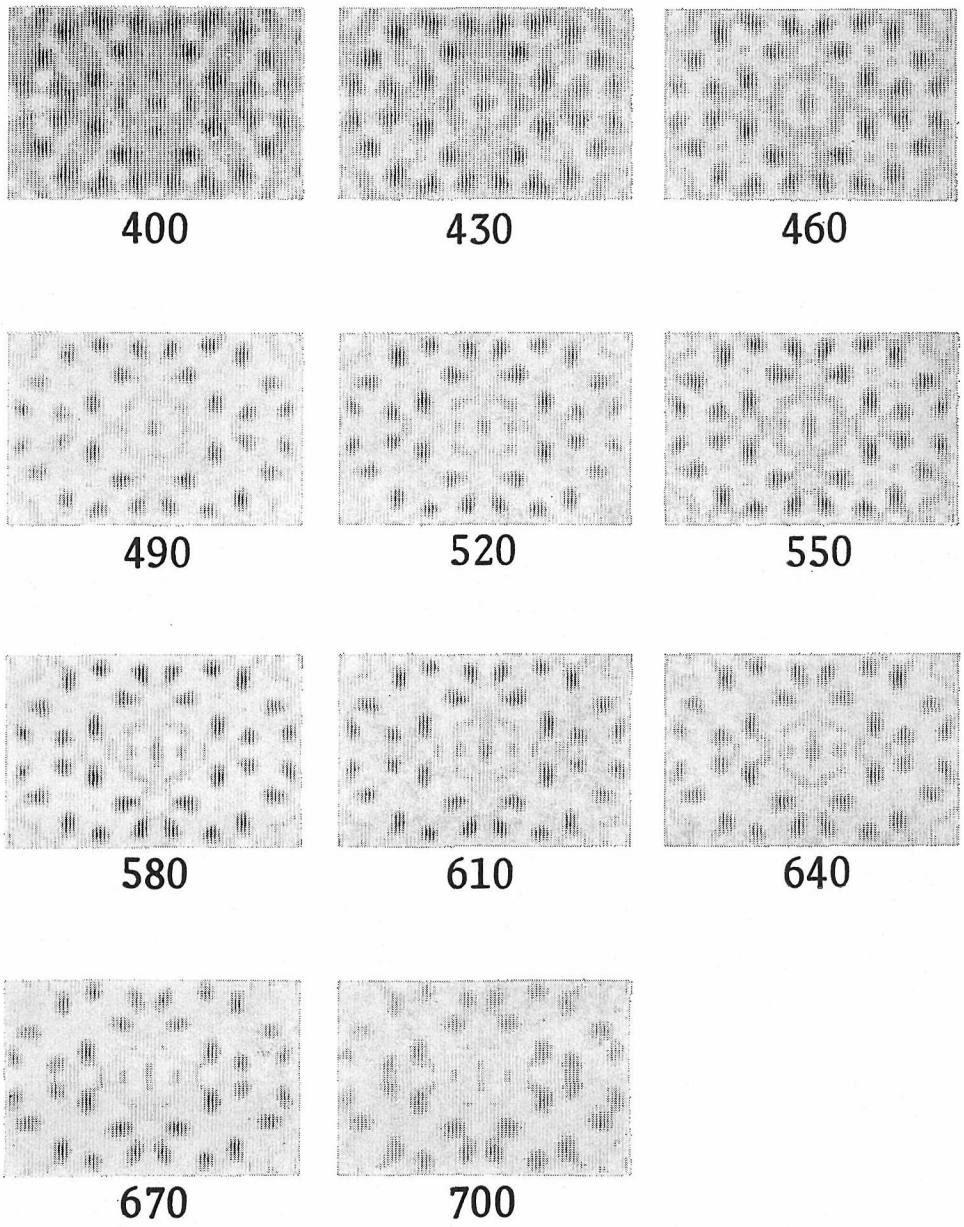


Fig. 7. Simulated molecular images of the bright field mode in the vicinity of the best focus with $C_s$=1.8 mm for 500 kV electrons. The heavy atoms are clearly observed, while the *iso*-indole rings are slightly deformed at the defocuses between 460 and 610 Å.

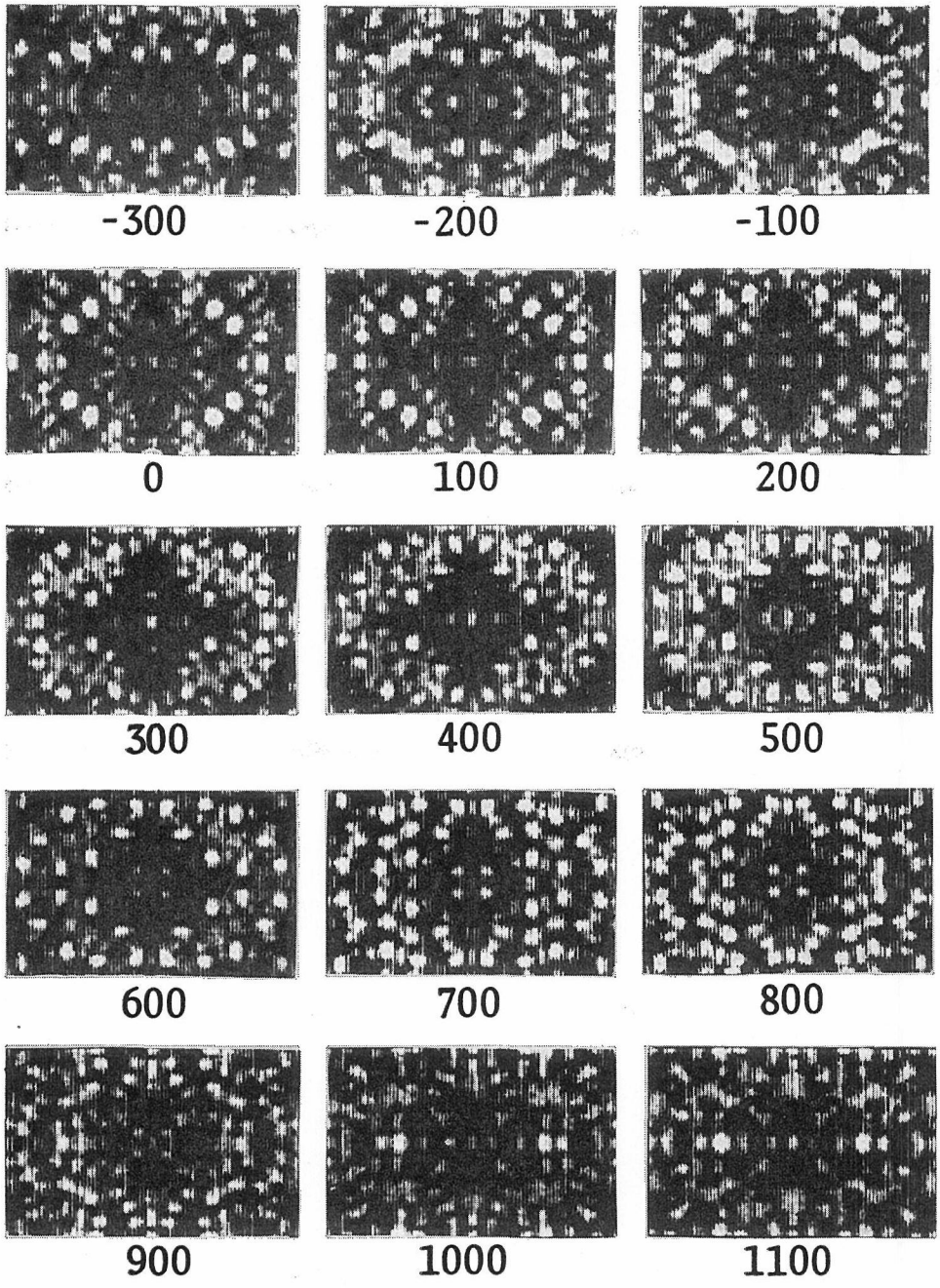


Fig. 8. Simulated images of the dark field mode with $C_s$=1.8 mm for 500 kV electrons ($s_{min}$=0.01 and $s_{max}$=0.264 Å$^{-1}$). The best image is obtained at the defocus value between 500 and 600 Å.

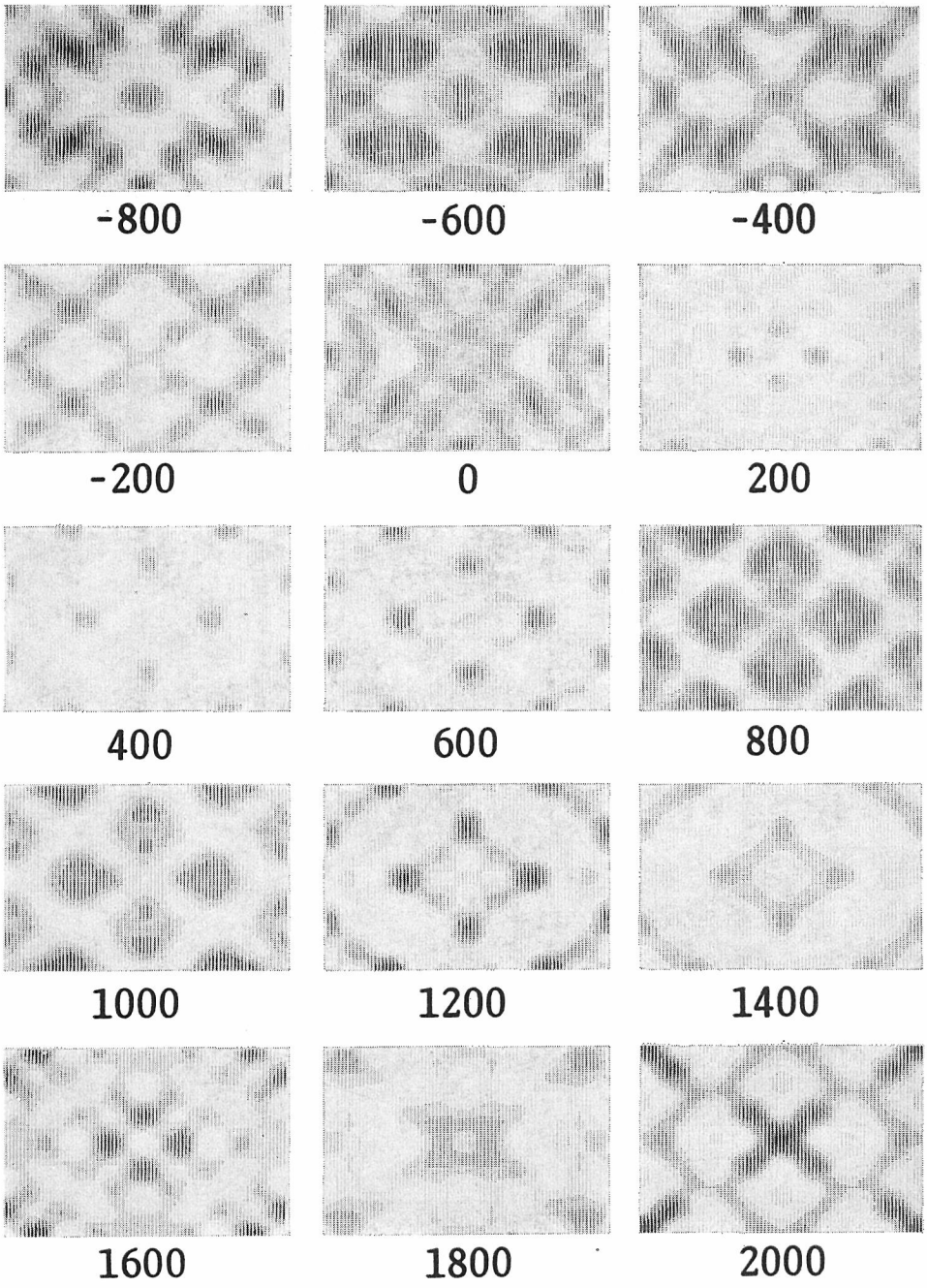


Fig. 9. Simulated images of the bright field mode with $C_s$=1.4 mm for 100 kV electrons ($s_{max}$=0.146 Å$^{-1}$). Only the molecular shape like a four-leaf clover can be observed even at the best focus of about 900 Å.

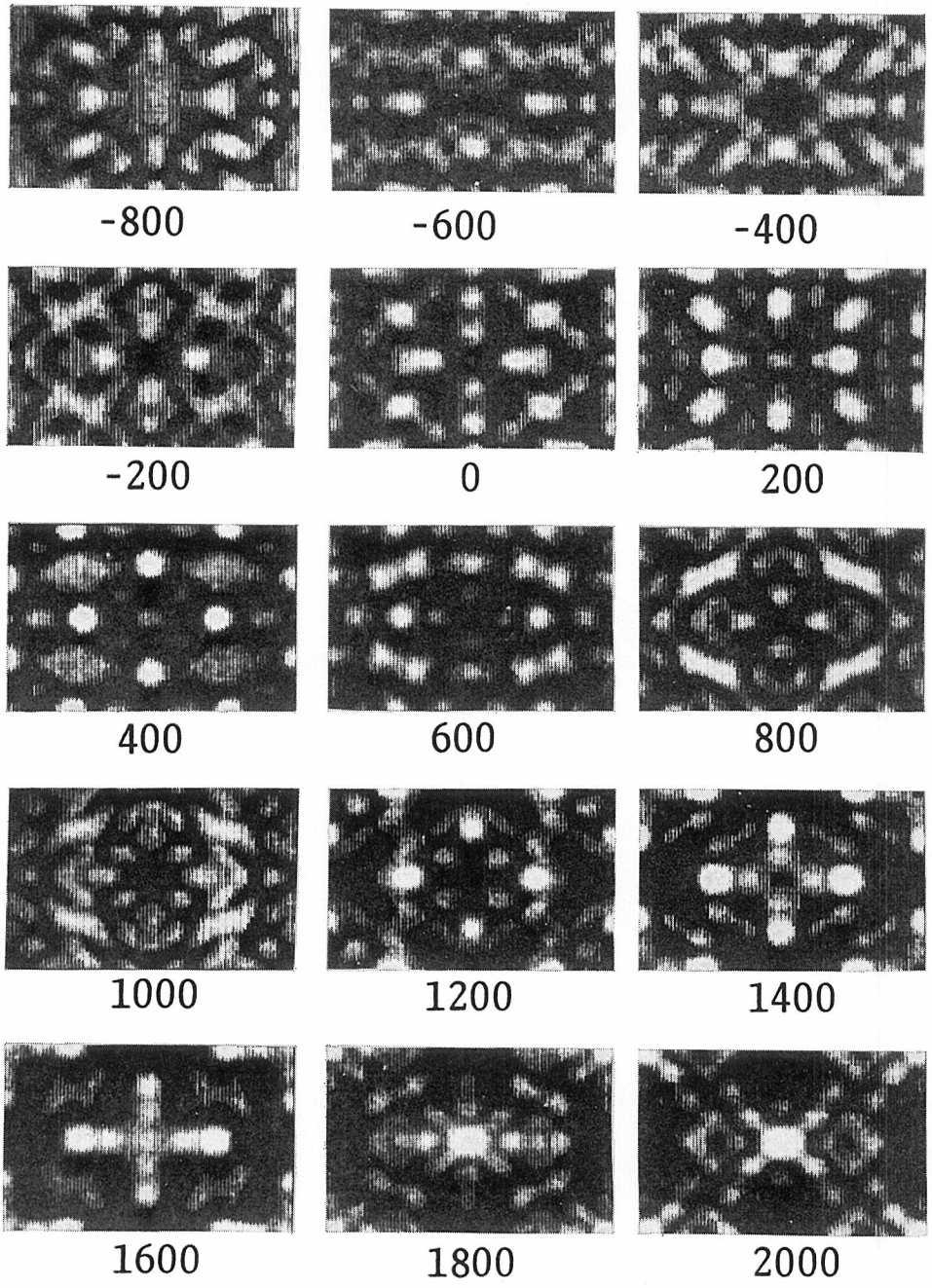


Fig. 10. Simulated images of the dark field mode with $C_s$=1.4 mm for 100 kV electrons ($s_{min}$=0.01 and $s_{max}$=0.146 Å$^{-1}$). Even at the best focus (900 Å), the ghost peaks are greater than the molecular components of the four-leaf clover.

field mode, while the observation of the molecular details is difficult in the dark field mode even for the 500 kV electrons, and that the dark field images for 100 kV electrons are inferior to the bright field ones for the observation of the molecular specimens in contrast to the case of isolated atoms.[2,5] It may be not easy to take a micrograph of molecular details, because it will appear only at one focus position in through-focusing series in both the bright and the dark field modes. A method to overcome this difficulty has been proposed elsewhere.[22]

## ACKNOWLEDGMENTS

The authors wish to thank Professor K. Kobayashi for his kind criticism and discussion. This paper is dedicated to Emeritus Professor E. Suito on the commemoration of his retirement.

## REFERENCES

(1) E. Ruska, "Electron Microscopy," Academic Press, New York, Proc. Fifth Intern'l Congr. for Electron Microscopy, Philadelphia, **1**, A–1 (1962).
(2) H. Hashimoto, A. Kumao, K. Hino, H. Yotsumoto, and A. Ono, *Japan. J. Appl. Phys.*, **10**, 1115 (1971).
(3) H. Formanek, M. Müller, M. H. Hahn, and Th. Koller, *Naturwissenschaften*, **58**, 339 (1971).
(4) J. R. Parsons and H. M. Johnson, C. W. Hoelke and R. P. Hosbons, *Phil. Mag.*, **27**, 1359 (1973).
(5) R. F. Whiting and F. P. Ottensmyer, *J. Mol. Biol.*, **67**, 173 (1972).
(6) N. Uyeda, T. Kobayashi, E. Suito, Y. Harada, and M. Watanabe, *J. Appl. Phys.*, **43**, 5181 (1972).
(7) J. M. Cowley and S. Iijima, *Z. Naturforsch.*, **27***a*, 445 (1972).
(8) S. Iijima, *Acta Cryst.*, *A***29**, 18 (1973).
(9) J. G. Allpress, E. A. Hewat, A. F. Moodie, and J. V. Sanders, *Acta Cryst.*, *A***28**, 536 (1972).
(10) O. Scherzer, *J. Appl. Phys.*, **20**, 20 (1949).
(11) C. B. Eisenhandler and B. M. Siegel, *J. Appl. Phys.*, **37**, 1613 (1966).
(12) D. L. Misell, *J. Phys. A* **6**, 62 (1973).
(13) N. Uyeda and K. Ishizuka, *J. Electron Microscopy*, **23**, 79 (1974).
(14) B. M. Siegel, *Ber. Bunsen-Ges. Physik. Chem.*, **74**, 1175 (1970).
(15) M. A. O'Keefe, *Acta Cryst.*, *A***29**, 389 (1973).
(16) J. M. Cowley, *Acta Cryst.*, *A***29**, 529 (1973).
(17) J. M. Cowley and A. F. Moodie, *Acta Cryst.*, **10**, 609 (1957).
(18) K. Kobayashi, E. Suito, N. Uyeda, M. Watanabe, T. Yanaka, T. Etoh, H. Watanabe, and M. Moriguchi, *Proc. Eighth Intern'l Congr. Electron Micros., Canberra*, **1**, 30 (1974).
(19) M. Born and E. Wolf, "Principle of Optics," 4th ed., Pergamon Press, Inc., New York, (1970), p. 468.
(20) P. A. Doyle and P. S. Turner, *Acta Cryst.*, *A***24**, 390 (1968).
(21) K. Kobayashi and N. Uyeda, *Proc. Eighth Intern'l Congr. Electron Micros., Canberra*, **1**, 264 (1974).
(22) N. Uyeda and K. Ishizuka, *J. Electron Micros.* **24**, 65 (1975).